Physically motivated rank constraint on direct throughput of state-space models

Citation for the original published paper (version of record):
Gibanica, M., Abrahamsson, T., McKelvey, T. (2018)
Physically motivated rank constraint on direct throughput of state-space models
IFAC-PapersOnLine, 51(15): 341-346
http://dx.doi.org/10.1016/j.ifacol.2018.09.156

Available online at www.sciencedirect.com

ScienceDirect

IFAC PapersOnLine 51-15 (2018) 329–334

Physically motivated rank constraint on direct throughput of state-space models

Mladen Gibanica *,** Thomas J.S. Abrahamsson * Tomas McKelvey ***

* *Department of Mechanics and Maritime Sciences, Chalmers University of Technology, SE-412 96 Göteborg, Sweden (e-mail: mladen.gibanica@chalmers.se)*
** *Volvo Car Corporation, SE-405 31 Göteborg, Sweden*
*** *Department of Electrical Engineering, Chalmers University of Technology, SE-412 96 Göteborg, Sweden*

Abstract: In frequency range vibration testing a few outside band eigenmodes are often included in the system identification to compensate for residual mass and stiffness influences. It has been observed that, in particular, energy conjugate input-output pair transfer functions with strong outside band modes tend to render models with poor fit even after inclusion of mass and stiffness residuals. For such problems the inclusion of another complementary residual term has been found to improve the fit to data. In this paper, modal models identified from acceleration data with a subspace state-space method are considered. The residual mass influence is modelled with a state-space direct throughput while the stiffness and complementary residuals are modelled with extra states. Furthermore, for state-space models on accelerance form it is shown that the direct throughput matrix can be partitioned into a flexible and rigid motion partition. For systems with more inputs and outputs than rigid body modes it is shown that the rigid body motion partition has a bounded rank. The upper bound is equal to the number of rigid body modes. Therefore, for identified models on accelerance form this constraint must be enforced for physical consistency. The proposed method is applied on simulated finite element test data from an automotive component.

Keywords: System identification, subspace methods, residuals, mechanical systems, rank constraint, physical models, automotive industry

1. INTRODUCTION

In the automotive industry, and especially in the noise vibration and harshness (NVH) field, system identification Ljung (1999) is often used for finite element (FE) model updating and validation, see e.g. Abrahamsson and Kammer (2015). It is also used for obtaining experimental models of hard-to-model components for use in coupling with experimental-analytical substructuring techniques, see Sjövall and Abrahamsson (2007); Liljerehn (2016). Very good identified models are essential in both situations, and in the latter case physically consistent models are also necessary for success. Commonly, accelerances are measured in most vibration testing because of the ease of use and cost benefits of using accelerometers. For coupling applications, specific degrees-of-freedom (DOFs) are used for coupling at which the direct accelerances (acceleration related to force at the same location and orientation in an energy conjugated pair) must be known. It is therefore common practice to perform experiments with inputs and outputs at all coupling locations. For successful coupling good models of the direct accelerances are absolutely necessary along with physically consistent models. In this paper both problems are addressed.

In frequency based system identification a frequency region of interest is selected. For continuous systems, with infinitely many modes, most high frequency modes above the cut-off frequency are only marginally observable in test data. Such modes give a more-or-less quadratic contribution to accelerance data in the frequency region of interest. Therefore, it is common to augment the identified model with a residual stiffness term with pseudo quadratic behaviour to compensate for these modes, see Ewins (2000). Furthermore, for systems with quasi-free boundary conditions, i.e. structures tested on soft supports, quasi-rigid body motion at low frequencies are present. These are usually below the cut-on frequency, giving a more-or-less constant contribution in the frequency region of interest. Such identified models are therefore augmented with an additional mass residual with constant behaviour, see Ewins (2000). However, for structures with strong local modes just outside the tested frequency range, it has been observed that direct accelerances are estimated poorly even after inclusion of the residual mass and stiffness terms. This problem has been addressed in Gibanica et al. (2018) where a procedure is proposed, based on the frequency domain subspace state-space system identification method N4SID McKelvey et al. (1996). The procedure includes a complementary residual, improving the direct accelerance model fit without affecting the cross-accelerances significantly. Mass and stiffness residual terms, consistent with a state-space description, are used together with a

Peer review under responsibility of International Federation of Automatic Control.
10.1016/j.ifacol.2018.09.156

complementary residual term that compensates for strong local modes just above the frequency range of interest to improve the identified model. Two strategies are proposed for the the complementary residual term's pole placement. However, in that procedure only the single-input multiple output (SIMO) case is treated and no physical consistency is imposed on the identified model. It should be mentioned that previous research has addressed various physical constraints in models identified with N4SID McKelvey et al. (1996) which can be found in McKelvey and Reza Moheimani (2005); Sjövall et al. (2006); Liljerehn (2016).

In this paper the procedure presented in Gibanica et al. (2018) is extended to continuous systems with rigid body modes for the multi-input multi-output (MIMO) case. The characteristic of a system with rigid-body modes is that it has multiple poles clustered at zero. It is possible to identify all rigid body modes when more inputs and outputs than rigid body modes are used in the test to render the system controllable and observable. It will here be shown that the direct throughput matrix for such systems must be rank constrained for physical consistency. However, first it is shown that a decomposition of the throughput matrix is possible where one part relates to flexible body modes, denoted the flexible part, and another to rigid body modes, denoted the rigid part. Further, it is shown that the rigid part of the direct throughput matrix models the rigid body modes completely for systems identified on accelerance test data. For continuous systems a modal truncation is inevitably performed when the frequency band is selected resulting in a contaminated rigid part of the throughput matrix. The contamination manifests as a full rank rigid partition of the throughput matrix, which for physical consistency should have rank equal to the number of rigid body modes. The rank constraint on the rigid partition of the direct throughput matrix is imposed through a truncated singular value decomposition (SVD) in a linear least-squares estimation of the rigid partition from an initially identified system. Models are estimated on simulated data from an FE model from a rear subframe of the Volvo XC90 (2015), see Gibanica and Abrahamsson (2017).

The theory is presented in Section 2 with Section 2.1 and 2.3 presenting the novelty of the paper; namely the direct throughput matrix decomposition and its rank constraint, respectively. In Section 3 the results are presented and Section 4 concludes the paper.

2. THEORY

First a description of the direct throughput matrix decomposition is given, followed by pre-processing steps on test data and model identification. Finally, model post-processing and the rank constraint are described.

2.1 Decomposition of direct throughput matrix

A linear mechanical system with m_r rigid body modes and m_f flexible modes can be modelled on first order form

$$\dot{\boldsymbol{x}}(t) = \boldsymbol{A}\boldsymbol{x}(t) + \boldsymbol{B}\boldsymbol{u}(t) \tag{1a}$$
$$\boldsymbol{y}_\mathrm{d}(t) = \boldsymbol{C}_\mathrm{d}\boldsymbol{x}(t) \tag{1b}$$

where $\boldsymbol{x} \in \mathcal{R}^{n\times 1}$ is the state vector, $\boldsymbol{u} \in \mathcal{R}^{n_\mathrm{u}\times 1}$ is the input vector and $\boldsymbol{y}_\mathrm{d} \in \mathcal{R}^{n_\mathrm{y}\times 1}$ is the displacement output vector, with $n = n_\mathrm{r} + n_\mathrm{f}$, n_u and n_y denoting the number of system states, inputs and outputs, respectively. The relations $n_\mathrm{r} = 2m_\mathrm{r}$ and $n_\mathrm{f} = 2m_\mathrm{f}$ hold. Here $\boldsymbol{A}$, $\boldsymbol{B}$ and $\boldsymbol{C}_\mathrm{d}$ are the system, input and displacement output matrices, respectively. Explicit time dependence is here on dropped for brevity. Velocity outputs can be obtained as

$$\begin{aligned}\boldsymbol{y}_\mathrm{v} = \dot{\boldsymbol{y}}_\mathrm{d} &= \boldsymbol{C}_\mathrm{d}\dot{\boldsymbol{x}} = \boldsymbol{C}_\mathrm{d}\left(\boldsymbol{A}\boldsymbol{x} + \boldsymbol{B}\boldsymbol{u}\right)\\ &= \boldsymbol{C}_\mathrm{d}\boldsymbol{A}\boldsymbol{x} + \boldsymbol{C}_\mathrm{d}\boldsymbol{B}\boldsymbol{u} \triangleq \boldsymbol{C}_\mathrm{v}\boldsymbol{x}\end{aligned} \tag{2}$$

with $\boldsymbol{C}_\mathrm{v}$ the velocity output matrix. Note that $\boldsymbol{C}_\mathrm{d}\boldsymbol{B} = \boldsymbol{0}$ on physical ground since there is no direct relation between velocity and force stimulus. Acceleration outputs may be obtained as

$$\begin{aligned}\boldsymbol{y} = \dot{\boldsymbol{y}}_\mathrm{v} &= \boldsymbol{C}_\mathrm{v}\dot{\boldsymbol{x}} = \boldsymbol{C}_\mathrm{v}\left(\boldsymbol{A}\boldsymbol{x} + \boldsymbol{B}\boldsymbol{u}\right)\\ &= \boldsymbol{C}_\mathrm{v}\boldsymbol{A}\boldsymbol{x} + \boldsymbol{C}_\mathrm{v}\boldsymbol{B}\boldsymbol{u} = \boldsymbol{C}_\mathrm{d}\boldsymbol{A}^2\boldsymbol{x} + \boldsymbol{C}_\mathrm{d}\boldsymbol{A}\boldsymbol{B}\boldsymbol{u}\\ &\triangleq \boldsymbol{C}\boldsymbol{x} + \boldsymbol{D}\boldsymbol{u}\end{aligned} \tag{3}$$

where $\boldsymbol{C}$ is the acceleration output matrix and $\boldsymbol{D}$ is the accelerance direct throughput matrix. This results in the well known state-space system.

$$\dot{\boldsymbol{x}} = \boldsymbol{A}\boldsymbol{x} + \boldsymbol{B}\boldsymbol{u} \tag{4a}$$
$$\boldsymbol{y} = \boldsymbol{C}\boldsymbol{x} + \boldsymbol{D}\boldsymbol{u} \tag{4b}$$

This system can be brought to Jordan normal form, Horn and Johnson (2012), using $\boldsymbol{A}\boldsymbol{T} = \boldsymbol{T}\boldsymbol{\Lambda}$ and $\boldsymbol{z} = \boldsymbol{T}\boldsymbol{x}$

$$\dot{\boldsymbol{z}} = \boldsymbol{\Lambda}\boldsymbol{z} + \bar{\boldsymbol{B}}\boldsymbol{u} \tag{5a}$$
$$\boldsymbol{y} = \bar{\boldsymbol{C}}\boldsymbol{z} + \boldsymbol{D}\boldsymbol{u} \tag{5b}$$

with $\boldsymbol{\Lambda} = \boldsymbol{T}^{-1}\boldsymbol{A}\boldsymbol{T}$, $\bar{\boldsymbol{B}} = \boldsymbol{T}^{-1}\boldsymbol{B}$ and $\bar{\boldsymbol{C}} = \boldsymbol{C}\boldsymbol{T}$. The system has eigenvalues $\lambda_r = 0$ with multiplicity n_r and n_f non-zero eigenvalues λ_f. The states can therefore be partitioned as $\boldsymbol{z} = \left[\boldsymbol{z}_\mathrm{r}^\mathrm{T}, \boldsymbol{z}_\mathrm{f}^\mathrm{T}\right]^\mathrm{T}$, with subscripts r and f denoting the rigid body and flexible body states, respectively. The system, input and output matrices are then partitioned as

$$\boldsymbol{\Lambda} = \begin{bmatrix}\boldsymbol{\Lambda}_\mathrm{r} & \boldsymbol{0}\\ \boldsymbol{0} & \boldsymbol{\Lambda}_\mathrm{f}\end{bmatrix}, \quad \bar{\boldsymbol{B}} = \begin{bmatrix}\bar{\boldsymbol{B}}_\mathrm{r}\\ \bar{\boldsymbol{B}}_\mathrm{f}\end{bmatrix} \quad \text{and} \quad \bar{\boldsymbol{C}} = \left[\bar{\boldsymbol{C}}_\mathrm{r}\ \bar{\boldsymbol{C}}_\mathrm{f}\right]. \tag{6}$$

Here $\boldsymbol{\Lambda}_\mathrm{r} \in \mathcal{R}^{n_\mathrm{r}\times n_\mathrm{r}}$ is Jordan, and real since it contains only zeros along the diagonal and ones along every second superdiagonal entry, and $\boldsymbol{\Lambda}_\mathrm{f} \in \mathcal{C}^{n_\mathrm{f}\times n_\mathrm{f}}$ is Jordan. Hence,

$$\begin{aligned}\boldsymbol{y} &= \left[\bar{\boldsymbol{C}}_\mathrm{d,r}\ \bar{\boldsymbol{C}}_\mathrm{d,f}\right]\begin{bmatrix}\boldsymbol{\Lambda}_\mathrm{r} & \boldsymbol{0}\\ \boldsymbol{0} & \boldsymbol{\Lambda}_\mathrm{f}\end{bmatrix}^2\begin{bmatrix}\boldsymbol{z}_\mathrm{r}\\ \boldsymbol{z}_\mathrm{f}\end{bmatrix}\\ &+ \left[\bar{\boldsymbol{C}}_\mathrm{d,r}\ \bar{\boldsymbol{C}}_\mathrm{d,f}\right]\begin{bmatrix}\boldsymbol{\Lambda}_\mathrm{r} & \boldsymbol{0}\\ \boldsymbol{0} & \boldsymbol{\Lambda}_\mathrm{f}\end{bmatrix}\begin{bmatrix}\bar{\boldsymbol{B}}_\mathrm{r}\\ \bar{\boldsymbol{B}}_\mathrm{f}\end{bmatrix}\boldsymbol{u}\\ &= \bar{\boldsymbol{C}}_\mathrm{d,r}\boldsymbol{\Lambda}_\mathrm{r}^2\boldsymbol{z}_\mathrm{r} + \bar{\boldsymbol{C}}_\mathrm{d,f}\boldsymbol{\Lambda}_\mathrm{f}^2\boldsymbol{z}_\mathrm{f}\\ &+ \left(\bar{\boldsymbol{C}}_\mathrm{d,r}\boldsymbol{\Lambda}_\mathrm{r}\bar{\boldsymbol{B}}_\mathrm{r} + \bar{\boldsymbol{C}}_\mathrm{d,f}\boldsymbol{\Lambda}_\mathrm{f}\bar{\boldsymbol{B}}_\mathrm{f}\right)\boldsymbol{u}\\ &\triangleq \bar{\boldsymbol{C}}_\mathrm{r}\boldsymbol{z}_\mathrm{r} + \bar{\boldsymbol{C}}_\mathrm{f}\boldsymbol{z}_\mathrm{f} + \left(\boldsymbol{D}_\mathrm{r} + \boldsymbol{D}_\mathrm{f}\right)\boldsymbol{u}\\ &\triangleq \bar{\boldsymbol{C}}_\mathrm{f}\boldsymbol{z}_\mathrm{f} + \boldsymbol{D}\boldsymbol{u}.\end{aligned} \tag{7}$$

The last equality holds because $\boldsymbol{\Lambda}_\mathrm{r}$ is a nilpotent matrix of degree 2, see Horn and Johnson (2012), and hence $\bar{\boldsymbol{C}}_\mathrm{r} = \boldsymbol{0}$. The system in (5) can be brought to frequency domain

$$\begin{aligned}\boldsymbol{G}(\omega) &= \bar{\boldsymbol{C}}\left(i\omega\boldsymbol{I} - \boldsymbol{\Lambda}\right)^{-1}\bar{\boldsymbol{B}} + \boldsymbol{D}\\ &= \bar{\boldsymbol{C}}_\mathrm{r}\left(i\omega\boldsymbol{I} - \boldsymbol{\Lambda}_\mathrm{r}\right)^{-1}\bar{\boldsymbol{B}}_\mathrm{r}\\ &+ \bar{\boldsymbol{C}}_\mathrm{f}\left(i\omega\boldsymbol{I} - \boldsymbol{\Lambda}_\mathrm{f}\right)^{-1}\bar{\boldsymbol{B}}_\mathrm{f} + \boldsymbol{D}\end{aligned} \tag{8}$$

with $i^2 = -1$ defining the imaginary number, ω the angular frequency and $\boldsymbol{G} \in \mathcal{C}^{n_\mathrm{y}\times n_\mathrm{u}}$ the frequency response function (FRF) matrix. For $\omega \neq 0$ $(i\omega\boldsymbol{I} - \boldsymbol{\Lambda}_\mathrm{r})$ is invertible because $\boldsymbol{\Lambda}_\mathrm{r}^2 = \boldsymbol{0}$. Further, for $\omega \to 0$ and with $\bar{\boldsymbol{C}}_\mathrm{r} = \boldsymbol{0}$

$$\lim_{\omega\to 0}\boldsymbol{G}(\omega) = -\bar{\boldsymbol{C}}_\mathrm{f}\boldsymbol{\Lambda}_\mathrm{f}^{-1}\bar{\boldsymbol{B}}_\mathrm{f} + \boldsymbol{D}. \tag{9}$$

We know that, see (7), the rigid body contribution to $\boldsymbol{D}$ is $\boldsymbol{D}_\mathrm{r} = \boldsymbol{D} - \boldsymbol{D}_\mathrm{f}$ and that

$$\boldsymbol{D}_\mathrm{f} = \bar{\boldsymbol{C}}_{\mathrm{d,f}}\boldsymbol{\Lambda}_\mathrm{f}\bar{\boldsymbol{B}}_\mathrm{f} = \bar{\boldsymbol{C}}_{\mathrm{d,f}}\boldsymbol{\Lambda}_\mathrm{f}^2\boldsymbol{\Lambda}_\mathrm{f}^{-1}\bar{\boldsymbol{B}}_\mathrm{f} = \bar{\boldsymbol{C}}_\mathrm{f}\boldsymbol{\Lambda}_\mathrm{f}^{-1}\bar{\boldsymbol{B}}_\mathrm{f}. \quad (10)$$

Hence, in the static case $\omega = 0$ we have

$$\boldsymbol{G}(0) = -\bar{\boldsymbol{C}}_\mathrm{f}\boldsymbol{\Lambda}_\mathrm{f}^{-1}\bar{\boldsymbol{B}}_\mathrm{f} + \boldsymbol{D} = \boldsymbol{D}_\mathrm{r}. \quad (11)$$

Interestingly, because $\bar{\boldsymbol{C}}_\mathrm{r} = \boldsymbol{0}$, the rigid body modes contribution to acceleration output only occur via the direct throughput matrix $\boldsymbol{D}$. Hence, systems identified from acceleration data need not include states corresponding to rigid body modes in $\boldsymbol{A}$ and only n_f states are required. This will be utilised in Section 2.2 and 2.3. However, for velocity or displacement outputs rigid body states need to be represented in $\boldsymbol{A}$. The following two lemmas regard the rank of $\boldsymbol{G}(0) = \boldsymbol{D}_\mathrm{r}$.

Lemma 1. Given $\boldsymbol{A} \in \mathcal{R}^{n\times n}$ with m_r rigid body modes and m_f flexible modes with $n = 2(m_\mathrm{r} + m_\mathrm{f})$, and $\boldsymbol{B} \in \mathcal{R}^{n\times n_\mathrm{u}}$ and $\boldsymbol{C} \in \mathcal{R}^{n_\mathrm{y}\times n}$, both full rank, then $\mathrm{rank}(\boldsymbol{D}_\mathrm{r}) = \min(m_\mathrm{r}, n_\mathrm{y}, n_\mathrm{u})$.

Proof. By definition of the Jordan $\boldsymbol{\Lambda}_\mathrm{r}$ $\mathrm{rank}(\boldsymbol{\Lambda}_\mathrm{r}) = m_\mathrm{r}$, therefore by construction $\mathrm{rank}(\boldsymbol{D}_\mathrm{r}) = \min(m_\mathrm{r}, n_\mathrm{y}, n_\mathrm{u})$. ■

Lemma 2. With model reduction of $n_{\mathrm{f},0}$ flexible modes of the system in Lemma 1 with $n_\mathrm{f} = n_{\mathrm{f},1} + n_{\mathrm{f},0}$ and $n_\mathrm{y}, n_\mathrm{u} > m_\mathrm{r}$, then $\mathrm{rank}(\boldsymbol{D}_\mathrm{r}) \leq \min(m_\mathrm{r}, n_\mathrm{y}, n_\mathrm{u}) + \min(n_{\mathrm{f},0}, n_\mathrm{y}, n_\mathrm{u})$.

Proof. $\boldsymbol{D}$ is unaffected by a modal truncation. Note that

$$\boldsymbol{D}_\mathrm{f} = \boldsymbol{D}_{\mathrm{f},1} + \boldsymbol{D}_{\mathrm{f},0} = \begin{bmatrix}\bar{\boldsymbol{C}}_{\mathrm{f},1} & \bar{\boldsymbol{C}}_{\mathrm{f},0}\end{bmatrix} \begin{bmatrix}\boldsymbol{\Lambda}_{\mathrm{f},1}^{-1} & \boldsymbol{0} \\ \boldsymbol{0} & \boldsymbol{\Lambda}_{\mathrm{f},0}^{-1}\end{bmatrix} \begin{bmatrix}\bar{\boldsymbol{B}}_{\mathrm{f},1} \\ \bar{\boldsymbol{B}}_{\mathrm{f},0}\end{bmatrix} \quad (12)$$

with $\boldsymbol{\Lambda}_{\mathrm{f},0}^{-1}$ the partition to be reduced. After reduction

$$\boldsymbol{D}_\mathrm{r} = \boldsymbol{D} - \boldsymbol{D}_{\mathrm{f},1} = \bar{\boldsymbol{C}}_{\mathrm{d,r}}\boldsymbol{\Lambda}_\mathrm{r}\bar{\boldsymbol{B}}_\mathrm{r} + \bar{\boldsymbol{C}}_{\mathrm{f},0}\boldsymbol{\Lambda}_{\mathrm{f},0}^{-1}\bar{\boldsymbol{B}}_{\mathrm{f},0} \quad (13)$$

and $\mathrm{rank}(\boldsymbol{D}_\mathrm{r}) \leq \min(m_\mathrm{r}, n_\mathrm{y}, n_\mathrm{u}) + \min(n_{\mathrm{f},0}, n_\mathrm{y}, n_\mathrm{u})$. ■

From Lemma 2 it follows that for truncated systems $\mathrm{rank}(\boldsymbol{D}_\mathrm{r})$ is not strictly upper bounded by $\min(m_\mathrm{r}, n_\mathrm{y}, n_\mathrm{u})$. However, by definition of $\boldsymbol{D}_\mathrm{r}$ in (7) only rigid body motion should contribute to the static motion and therefore when $n_\mathrm{y}, n_\mathrm{u} > m_\mathrm{r}$ $\boldsymbol{D}_\mathrm{r}$ must be rank constrained for truncated systems. Section 2.3 describes such a constraint.

2.2 Pre-processing of test data and model identification

In Gibanica et al. (2018) a procedure was presented to identify models from augmented SIMO test data where mass, stiffness and complementary residual state influences had been removed. This procedure is briefly restated here and extended for the MIMO case.

Residual modes with poles outside the frequency range of interest can be used to approximate the out of range behaviour of an identified model, see Ewins (2000) for a thorough explanation. A receptance FRF matrix $\boldsymbol{H}^\mathrm{R}(\omega) \in \mathcal{C}^{n_\mathrm{y}\times n_\mathrm{u}}$ of a linear undamped system can be expressed in modal parameters, for $j = 1, \ldots, n_\mathrm{y}$ and $k = 1, \ldots, n_\mathrm{u}$, as

$$\begin{aligned} H_{jk}^\mathrm{R}(\omega) &= \sum_{r=1}^{N} \frac{R_{jk}^{(r)}}{\omega_r^2 - \omega^2} \\ &= \sum_{r=1}^{N} \left(\frac{R_{jk}^{(r)}/(2\omega_r)}{\omega_r - \omega} + \frac{R_{jk}^{(r)}/(2\omega_r)}{\omega_r + \omega} \right) \end{aligned} \quad (14)$$

where ω_r is the eigenfrequency of the rth mode in magnitude ordered sequence, $R_{jk}^{(r)}$ the residue factor for mode r and N is the modal order of the system. For continuous systems $N = \infty$. Equation (14) can be written on acceleration form $\boldsymbol{H}^\mathrm{A}(\omega)$ and split into

$$H_{jk}^\mathrm{A}(\omega) = -\sum_{r=1}^{n_1-1} \frac{\omega^2 R_{jk}^{(r)}}{\omega_r^2 - \omega^2} - \sum_{r=n_1}^{n_2} \frac{\omega^2 R_{jk}^{(r)}}{\omega_r^2 - \omega^2} - \sum_{r=n_2+1}^{N} \frac{\omega^2 R_{jk}^{(r)}}{\omega_r^2 - \omega^2} \quad (15)$$

with n_1 and n_2 corresponding to the lowest and highest eigenfrequency inside of the frequency range of interest, respectively. The first term is generally identified as the contribution from low frequency modes and the third term as the contributions from high frequency modes. For frequencies ω inside the frequency range of interest the series may be approximated as, see Ewins (2000),

$$H_{jk}^\mathrm{A}(\omega) \approx \frac{1}{M_{jk}^\mathrm{R}} - \sum_{r=n_1}^{n_2} \frac{\omega^2 R_{jk}^{(r)}}{\omega_r^2 - \omega^2} - \frac{\omega^2}{K_{jk}^\mathrm{R}} \quad (16)$$

where M_{jk}^R and K_{jk}^R are the mass and stiffness residuals, respectively. This formulation is related to a state-space description, see (4), with the mass residual, constant in frequency, being represented by the direct throughput matrix $\boldsymbol{D}$. The stiffness residual associated with fast modes, quadratic in frequency, can be represented with a pole placed at infinity. However, this is not consistent with a normal state-space description. The terms with fast modes may instead be approximated with $Q_{jk}^\mathrm{R}(\omega)$ such that

$$H_{jk}^\mathrm{A}(\omega) \approx \frac{1}{M_{jk}^\mathrm{R}} - \sum_{r=n_1}^{n_2} \frac{\omega^2 R_{jk}^{(r)}}{\omega_r^2 - \omega^2} - Q_{jk}^\mathrm{R}(\omega). \quad (17)$$

The stiffness residualisation is possible since

$$\sum_{r=n_2+1}^{N} \frac{\omega^2 R_{jk}^{(r)}}{\omega_r^2 - \omega^2} \approx \sum_{r=n_2+1}^{N} \frac{\omega^2 R_{jk}^{(r)}}{\omega_r^2} \triangleq \frac{\omega^2}{K_{jk}^\mathrm{R}} \quad (18)$$

for eigenfrequencies $\omega_r \gg \omega$. An alternative residualisation is possible by introducing $\omega_\mathrm{K} \gg \omega$ leading to

$$\begin{aligned} \sum_{r=n_2+1}^{N} \frac{\omega^2 R_{jk}^{(r)}}{\omega_r^2 - \omega^2} &= \sum_{r=n_2+1}^{N} \frac{\left(\omega_\mathrm{K}^2 - \omega^2\right)\omega^2 R_{jk}^{(r)}}{\left(\omega_r^2 - \omega^2\right)\left(\omega_\mathrm{K}^2 - \omega^2\right)} \\ &\approx \sum_{r=n_2+1}^{N} \frac{\omega_\mathrm{K}^2}{\omega_r^2} \frac{\omega^2 R_{jk}^{(r)}}{\omega_\mathrm{K}^2 - \omega^2} \triangleq \frac{\omega^2 R_{jk}^{(\mathrm{K})}}{\omega_\mathrm{K}^2 - \omega^2}. \end{aligned} \quad (19)$$

The fast mode term $Q_{jk}^\mathrm{R}(\omega)$ is proposed to be approximated with a two term residual series as

$$Q_{jk}^\mathrm{R}(\omega) \approx \frac{\omega^2 R_{jk}^{(\mathrm{S})}}{\omega_\mathrm{S}^2 - \omega^2} + \frac{\omega^2 R_{jk}^{(\mathrm{K})}}{\omega_\mathrm{K}^2 - \omega^2} \quad (20)$$

where the first term is associated with a pseudo-mode at ω_S with residue factors $R_{jk}^{(\mathrm{S})}$. The introduced mode is at frequency $\omega_\mathrm{S} > \overline{\omega}$ such that the corresponding term is quasi-linear in frequency over the frequency range of interest $[\underline{\omega}, \overline{\omega}]$. The pole placement strategy is described in Gibanica et al. (2018). The second term approximates the residual stiffness with residue factors $R_{jk}^{(\mathrm{K})}$ and $\overline{\omega} \ll \omega_\mathrm{K} < \infty$ which will render the term approximately quadratic over $[\underline{\omega}, \overline{\omega}]$ and consistent with a state-space description with states for a mode at very high frequencies ω_K. Hence, the system's FRFs can be approximated with the series

$$H_{jk}^{\mathrm{A}}(\omega) \approx \frac{1}{M_{jk}^{\mathrm{R}}} - \sum_{r=n_1}^{n_2} \frac{\omega^2 R_{jk}^{(r)}}{\omega_r^2 - \omega^2} - \frac{\omega^2 R_{jk}^{(\mathrm{S})}}{\omega_{\mathrm{S}}^2 - \omega^2} - \frac{\omega^2 R_{jk}^{(\mathrm{K})}}{\omega_{\mathrm{K}}^2 - \omega^2}. \tag{21}$$

Let $\underline{\boldsymbol{H}}^{\mathrm{A}}(\Omega_m) \in \mathcal{C}^{n_{\mathrm{y}} \times n_{\mathrm{u}}}$ denote the experimental accelerance FRFs of the generally damped system for discrete frequencies $\Omega_m \in [\underline{\omega}, \overline{\omega}]$ for $m = 1, \ldots, M$. A low-order model $\hat{\boldsymbol{H}}^{\mathrm{A,low}}(\Omega_m) \in \mathcal{R}^{n_{\mathrm{y}} \times n_{\mathrm{u}}}$ of the three residuals can be found from the real valued experimental data

$$\underline{\boldsymbol{H}}^{\mathrm{A,Re}}(\Omega_m) = \mathcal{R}\left(\underline{\boldsymbol{H}}^{\mathrm{A}}(\Omega_m)\right) \in \mathcal{R}^{n_{\mathrm{y}} \times n_{\mathrm{u}}}. \tag{22}$$

Hence, the residue factors $\alpha_{jk} = 1/M_{jk}^{\mathrm{R}}$, $\beta_{jk} = R_{jk}^{(\mathrm{S})}$ and $\gamma_{jk} = R_{jk}^{(\mathrm{K})}$ need to be determined. Let $\boldsymbol{\theta}_{jk} = [\alpha_{jk}, \beta_{jk}, \gamma_{jk}]^{\mathrm{T}}$ define the parameter vector and consider a linear least-squares solution Horn and Johnson (2012) for each individual channel $j = 1, \ldots, n_{\mathrm{y}}$ and $k = 1, \ldots, n_{\mathrm{u}}$

$$\hat{\boldsymbol{\theta}}_{jk} = \arg\min_{\boldsymbol{\theta}_{jk}} \left\| \underline{\boldsymbol{H}}_{jk}^{\mathrm{A,Re}} - \boldsymbol{E}\boldsymbol{\theta}_{jk} \right\|_{\mathrm{F}} \in \mathcal{R}^{3 \times 1} \tag{23}$$

with $\|\cdot\|_{\mathrm{F}}$ the Frobenius norm. Note that $\underline{\boldsymbol{H}}_{jk}^{\mathrm{A,Re}} \in \mathcal{R}^{M \times 1}$ is a vector containing one channel from the FRF matrix along the frequency dimension. Let data matrix $\boldsymbol{E}$ be

$$\boldsymbol{E} = \begin{bmatrix} 1 & \Omega_1^2/(\omega_{\mathrm{S}}^2 - \Omega_1^2) & \Omega_1^2/(\omega_{\mathrm{K}}^2 - \Omega_1^2) \\ 1 & \Omega_2^2/(\omega_{\mathrm{S}}^2 - \Omega_2^2) & \Omega_2^2/(\omega_{\mathrm{K}}^2 - \Omega_2^2) \\ \vdots & \vdots & \vdots \end{bmatrix} \in \mathcal{R}^{M \times 3} \tag{24}$$

which is full column rank since $\omega_{\mathrm{S}} \neq \omega_{\mathrm{K}}$. The solution $\hat{\boldsymbol{\theta}}_{jk}$ is obtained by the Moore-Penrose pseudoinverse $\boldsymbol{E}^+$ as

$$\hat{\boldsymbol{\theta}}_{jk} = \boldsymbol{E}^+ \underline{\boldsymbol{H}}_{jk}^{\mathrm{A,Re}} \tag{25}$$

and hence the estimated FRF matrix $\hat{\boldsymbol{H}}^{\mathrm{A,low}}(\Omega_m)$ can be obtained for each channel as

$$\hat{\boldsymbol{H}}_{jk}^{\mathrm{A,low}} = \boldsymbol{E}\hat{\boldsymbol{\theta}}_{jk} \in \mathcal{R}^{M \times 1}. \tag{26}$$

An augmented model $\bar{\boldsymbol{H}}^{\mathrm{A}}(\Omega_m)$ without the undamped residual model's contribution $\hat{\boldsymbol{H}}^{\mathrm{A,low}}(\Omega_m)$ is obtained by removing it from experimental data $\underline{\boldsymbol{H}}^{\mathrm{A}}(\Omega_m)$ for each frequency Ω_m as

$$\bar{\boldsymbol{H}}^{\mathrm{A}}(\Omega_m) = \underline{\boldsymbol{H}}^{\mathrm{A}}(\Omega_m) - \hat{\boldsymbol{H}}^{\mathrm{A,low}}(\Omega_m) \in \mathcal{C}^{n_{\mathrm{y}} \times n_{\mathrm{u}}}. \tag{27}$$

The N4SID method, implemented in MATLAB's System Identification Toolbox McKelvey et al. (1996), is used on this data, $\bar{\boldsymbol{H}}^{\mathrm{A}}(\Omega_m)$, to obtain the quadruple $\boldsymbol{\Sigma}^{\mathrm{id}} = \{\boldsymbol{A}^{\mathrm{id}}, \boldsymbol{B}^{\mathrm{id}}, \boldsymbol{C}^{\mathrm{id}}, \boldsymbol{D}^{\mathrm{id}}\}$ which represent the identified model on first order form.

It is possible to find a state-space representation of system $\hat{H}_{jk}^{\mathrm{A,low}}(\Omega_m = -is_m) = \boldsymbol{E}(\Omega_m)\hat{\boldsymbol{\theta}}_{jk}$ by writing the transfer functions on zero-pole gain form

$$\hat{H}_{jk}^{\mathrm{A,low}}(s_m) = q_{jk} \frac{(s_m - z_{jk,1})(s_m - z_{jk,2})(s_m - z_{jk,3})(s_m - z_{jk,4})}{(s_m - i\omega_{\mathrm{S}})(s_m + i\omega_{\mathrm{S}})(s_m - i\omega_{\mathrm{K}})(s_m + i\omega_{\mathrm{K}})} \tag{28}$$

where q_{jk} is the channel gain and $z_{jk,v}$ its zeros, with $v = \{1, 2, 3, 4\}$, found from $\hat{\boldsymbol{\theta}}_{jk}$. From the system zeros, poles and gains a state-space system $\boldsymbol{\Sigma}^{\mathrm{low}} = \{\boldsymbol{A}^{\mathrm{low}}, \boldsymbol{B}^{\mathrm{low}}, \boldsymbol{C}^{\mathrm{low}}, \boldsymbol{D}^{\mathrm{low}}\}$ can be found Kailath (1980). For the MIMO case system $\boldsymbol{\Sigma}^{\mathrm{low}}$ is constructed with two modes placed at ω_{K} and ω_{S} for each input. Hence the system has $4n_{\mathrm{u}}$ states.

2.3 Post-processing of identified model

To describe the original data $\underline{\boldsymbol{H}}_m^{\mathrm{A}} \triangleq \underline{\boldsymbol{H}}^{\mathrm{A}}(\Omega_m)$ the two identified systems $\boldsymbol{\Sigma}^{\mathrm{low}}$ and $\boldsymbol{\Sigma}^{\mathrm{id}}$ must be connected in parallel, producing system $\boldsymbol{\Sigma} = \{\boldsymbol{A}, \boldsymbol{B}, \boldsymbol{C}, \boldsymbol{D}\}$ with

$$\boldsymbol{A} = \begin{bmatrix} \boldsymbol{A}^{\mathrm{id}} & \boldsymbol{0} \\ \boldsymbol{0} & \boldsymbol{A}^{\mathrm{low}} \end{bmatrix}, \quad \boldsymbol{B} = \begin{bmatrix} \boldsymbol{B}^{\mathrm{id}} \\ \boldsymbol{B}^{\mathrm{low}} \end{bmatrix}, \quad \boldsymbol{C} = \begin{bmatrix} \boldsymbol{C}^{\mathrm{id}} & \boldsymbol{C}^{\mathrm{low}} \end{bmatrix} \quad \text{and} \quad \boldsymbol{D} = \boldsymbol{D}^{\mathrm{id}} + \boldsymbol{D}^{\mathrm{low}}. \tag{29}$$

For this system the $\{\boldsymbol{B}, \boldsymbol{C}, \boldsymbol{D}\}$ matrices are not necessarily optimal and therefore need to be re-estimated, see Gumussoy et al. (2018) for a theoretical treaty of the re-estimation problem. Here $\boldsymbol{\Sigma}$ is transformed to $\boldsymbol{\Sigma}_\Lambda = \{\boldsymbol{\Lambda}, \bar{\boldsymbol{B}}, \bar{\boldsymbol{C}}, \boldsymbol{D}\}$ using (5). In Section 2.1 it was stated that $\boldsymbol{D} = \boldsymbol{D}_{\mathrm{r}} + \boldsymbol{D}_{\mathrm{f}}$ and $\bar{\boldsymbol{C}}_{\mathrm{r}} = \boldsymbol{0}$. From (11) we know that the rigid body motion is modelled only in $\boldsymbol{D}_{\mathrm{r}}$ and hence from (10) $\boldsymbol{D}_{\mathrm{f}} = \bar{\boldsymbol{C}}\boldsymbol{\Lambda}^{-1}\bar{\boldsymbol{B}}$. Furthermore, Lemma 2 stated that $\boldsymbol{D}_{\mathrm{r}}$ is not necessarily upper bounded by $\min(m_{\mathrm{r}}, n_{\mathrm{y}}, n_{\mathrm{u}})$ for truncated systems. Hence, using a limited number of residual modes to compensate for truncated modes the resulting $\boldsymbol{D}_{\mathrm{r}}$ should be constrained to $\mathrm{rank}(\boldsymbol{D}_{\mathrm{r}}) = m_{\mathrm{r}}$ for physical consistency. From the frequency domain representation of $\boldsymbol{\Sigma}_\Lambda$

$$\begin{aligned} \boldsymbol{H}_m^{\mathrm{A},\Sigma_\Lambda} &= \bar{\boldsymbol{C}}\left(i\Omega_m\boldsymbol{I} - \boldsymbol{\Lambda}\right)^{-1}\bar{\boldsymbol{B}} + \boldsymbol{D}_{\mathrm{f}} + \boldsymbol{D}_{\mathrm{r}} \\ &= \bar{\boldsymbol{C}}\left(\left(i\Omega_m\boldsymbol{I} - \boldsymbol{\Lambda}\right)^{-1} + \boldsymbol{\Lambda}^{-1}\right)\bar{\boldsymbol{B}} + \boldsymbol{D}_{\mathrm{r}} \\ &\triangleq \bar{\boldsymbol{C}}\boldsymbol{Q}_m\bar{\boldsymbol{B}} + \boldsymbol{D}_{\mathrm{r}} \end{aligned} \tag{30}$$

a minimisation problem can be formulated

$$\underset{\substack{\bar{\boldsymbol{B}}, \bar{\boldsymbol{C}}, \boldsymbol{D}_{\mathrm{r}} \\ \text{s. t. } \mathrm{rank}(\boldsymbol{D}_{\mathrm{r}}) = m_{\mathrm{r}}}}{\arg\min} \sum_{m=1}^{M} \left\| \underline{\boldsymbol{H}}_m^{\mathrm{A}} - \boldsymbol{D}_{\mathrm{r}} - \bar{\boldsymbol{C}}\boldsymbol{Q}_m\bar{\boldsymbol{B}} \right\|_{\mathrm{F}}. \tag{31}$$

The transfer function in (30) is bilinear in $\{\bar{\boldsymbol{B}}, \bar{\boldsymbol{C}}, \boldsymbol{D}_{\mathrm{r}}\}$, i.e. linear in either $\{\bar{\boldsymbol{B}}, \boldsymbol{D}_{\mathrm{r}}\}$ or $\{\bar{\boldsymbol{C}}, \boldsymbol{D}_{\mathrm{r}}\}$ given $\boldsymbol{\Lambda}$. It is therefore possible to iteratively re-estimate $\bar{\boldsymbol{B}}$, $\bar{\boldsymbol{C}}$ and $\boldsymbol{D}_{\mathrm{r}}$ using a sequence of linear least-squares solutions until convergence is reached. The rank constraint on $\boldsymbol{D}_{\mathrm{r}}$ is imposed using the parametrisation

$$\boldsymbol{D}_{\mathrm{r}} \triangleq \boldsymbol{D}_{\mathrm{r,L}}\boldsymbol{D}_{\mathrm{r,R}} \tag{32}$$

where the two factors $\boldsymbol{D}_{\mathrm{r,L}}$ and $\boldsymbol{D}_{\mathrm{r,R}}$ have m_{r} columns and rows, respectively. We initialise this factorisation using an SVD of $\boldsymbol{D}_{\mathrm{r}} = \boldsymbol{U}\boldsymbol{S}\boldsymbol{V}^{\mathrm{T}}$, which can be partitioned as

$$\boldsymbol{D}_{\mathrm{r}} = [\boldsymbol{U}_{\mathrm{r}} \ \boldsymbol{U}_0] \begin{bmatrix} \boldsymbol{S}_{\mathrm{r}} & \boldsymbol{0} \\ \boldsymbol{0} & \boldsymbol{S}_0 \end{bmatrix} \begin{bmatrix} \boldsymbol{V}_{\mathrm{r}}^{\mathrm{T}} \\ \boldsymbol{V}_0^{\mathrm{T}} \end{bmatrix}. \tag{33}$$

In an ideal noise-free and non-truncated system the partition $\boldsymbol{S}_0 = \boldsymbol{0}$, but due to truncation and noise $\boldsymbol{S}_0 \neq \boldsymbol{0}$. Hence, with the m_{r} most significant singular values $\boldsymbol{S}_{\mathrm{r}}$ kept

$$\boldsymbol{D}_{\mathrm{r,L}} \triangleq \boldsymbol{U}_{\mathrm{r}}\sqrt{\boldsymbol{S}_{\mathrm{r}}} \quad \text{and} \quad \boldsymbol{D}_{\mathrm{r,R}} \triangleq \sqrt{\boldsymbol{S}_{\mathrm{r}}}\boldsymbol{V}_{\mathrm{r}}^{\mathrm{T}}. \tag{34}$$

Then, the sequence of linear least-squares solutions, outlined below, is iterated for $p = 0, \ldots, P-1$.

$$\bar{\boldsymbol{C}}^{p+1}, \boldsymbol{D}_{\mathrm{r,L}}^{p+1} = \underset{\bar{\boldsymbol{C}}, \boldsymbol{D}_{\mathrm{r,L}}}{\arg\min} \sum_{m=1}^{M} \left\| \underline{\boldsymbol{H}}_m^{\mathrm{A}} - \boldsymbol{D}_{\mathrm{r,L}}\boldsymbol{D}_{\mathrm{r,R}}^{p} - \bar{\boldsymbol{C}}\boldsymbol{Q}_m\bar{\boldsymbol{B}}^{p} \right\|_{\mathrm{F}} \tag{35a}$$

$$\bar{\boldsymbol{B}}^{p+1}, \boldsymbol{D}_{\mathrm{r,R}}^{p+1} = \underset{\bar{\boldsymbol{B}}, \boldsymbol{D}_{\mathrm{r,R}}}{\arg\min} \sum_{m=1}^{M} \left\| \underline{\boldsymbol{H}}_m^{\mathrm{A}} - \boldsymbol{D}_{\mathrm{r,L}}^{p+1}\boldsymbol{D}_{\mathrm{r,R}} - \bar{\boldsymbol{C}}^{p+1}\boldsymbol{Q}_m\bar{\boldsymbol{B}} \right\|_{\mathrm{F}} \tag{35b}$$

In a last step $\boldsymbol{D}^P$ is calculated as $\boldsymbol{D}^P = \bar{\boldsymbol{C}}^P\boldsymbol{\Lambda}^{-1}\bar{\boldsymbol{B}}^P + \boldsymbol{D}_{\mathrm{r,L}}^P\boldsymbol{D}_{\mathrm{r,R}}^P$.

3. RESULTS

Data from an FE model of car rear subframe is used, shown in Fig. 1 with the used input-output configuration. FRF data was simulated from 40 to 800 Hz with 0.5 Hz frequency stepping with added white noise. Here 26 outputs and 9 energy conjugated inputs are used. These inputs relates to output numbers $\{2, 5, 13, 14, 17, 19, 20, 25, 26\}$. A total of $m_\mathrm{f} = 43$ flexible modes are present in this frequency region and the model contains $m_\mathrm{r} = 6$ rigid body modes due to its free-free boundary condition. Further model details can be found in Gibanica and Abrahamsson (2017); Gibanica et al. (2018).

Here four models are identified with a direct throughput matrix. In Fig. 2 the sum of all FRF channels' magnitude is shown. It can be seen that the model without residuals and $n = 2m_\mathrm{f} = 86$ states N4SID has poorest fit, where the fit is especially bad below 400 Hz. However, this model did not have re-estimated $\{\boldsymbol{B}, \boldsymbol{C}, \boldsymbol{D}\}$ matrices. The model with 2 residuals for every input channel and in total $n = 104$ states N4SID$_2$, i.e. identified with the presented procedure but with mass and stiffness residuals only, gives much better model fit but with severe discrepancy to data below 150 Hz. The model with 3 residuals for every input channel and in total $n = 122$ states N4SID$_3$ and the same model with rank constrained $\boldsymbol{D}_\mathrm{r}$ N4SID$_3^\mathrm{r}$ produce very good results over the whole frequency region with minimal differences between the methods. Below 150 Hz N4SID$_3^\mathrm{r}$ seems to give a better fit, but closer inspection shows that this is in general not true, and model N4SID$_3$ give slightly better fit near antiresonances. The complementary residual was placed at $\omega_\mathrm{S} = 1.4\overline{\omega}$. Models N4SID$_2$ and N4SID$_3$ had re-estimated $\{\boldsymbol{B}, \boldsymbol{C}, \boldsymbol{D}\}$ matrices while N4SID$_3^\mathrm{r}$ had re-estimated $\{\boldsymbol{B}, \boldsymbol{C}, \boldsymbol{D}_\mathrm{r}\}$ matrices with $\boldsymbol{D}_\mathrm{f}$ calculated according to (10). In the first iteration for models N4SID$_2$, N4SID$_3$ and N4SID$_3^\mathrm{r}$ the least-squares loss function is decreased by 70.82%, 87.39% and 86.39% relative each model's initial model, respectively. After $P = 9$ iterations the respective loss functions further decreased to 71.50%, 87.91% and 87.88%. Note that N4SID$_3$ and N4SID$_3^\mathrm{r}$ have the same initial model, implying that a physically consistent model can be obtained almost without sacrificing any model fit.

The normalised root-mean-square error (NRMSE) is used to measure model fit and defined as

$$\xi_{jk} = 1 - \frac{\left\| \underline{\boldsymbol{H}}_{jk}^\mathrm{A} - \boldsymbol{H}_{jk}^{\mathrm{A},\Sigma} \right\|_2}{\left\| \underline{\boldsymbol{H}}_{jk}^\mathrm{A} - \mathrm{mean}\left(\underline{\boldsymbol{H}}_{jk}^\mathrm{A} \right) \right\|_2} \in \mathcal{R} \tag{36}$$

with $\boldsymbol{H}_{jk}^{\mathrm{A},\Sigma}$ denoting any of the identified models. The NRMSE can take values $-\infty \leq \xi_{jk} \leq 1$ with $\xi_{jk} = 1$ indicating perfect fit and $\xi_{jk} = -\infty$ a poor fit. In Fig. 3 the fit is shown for each channel for each model. White indicate perfect fit $\xi_{jk} = 1$ and black bad fit $\xi_{jk} \leq 0.5$. It can be seen that the direct accelerance for channels 13, 14, 17 and 19 are especially bad for N4SID. These channels are improved in N4SID$_2$, but channel 13 and 14 still have poor fit. This is improved upon in N4SID$_3$ and N4SID$_3^\mathrm{r}$.

The direct accelerance for channel 14 is shown in Fig. 4 for all 4 models. The phase error η_{jk} is calculated as

$$\eta_{jk}(\Omega_m) = \left| \angle \left(\boldsymbol{H}_{jk}^{\mathrm{A},\Sigma}(\Omega_m) / \underline{\boldsymbol{H}}_{jk}^\mathrm{A}(\Omega_m) \right) \right| \in [0^\circ, 180^\circ] \tag{37}$$

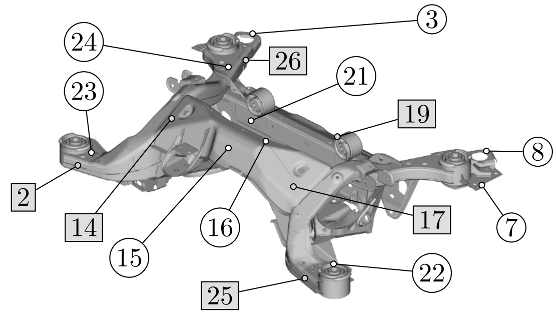

(a) Top view

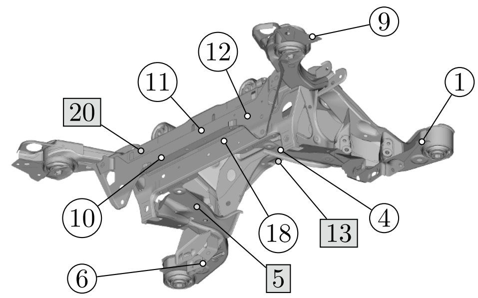

(b) Bottom view

Fig. 1. Top view of rear subframe in (a) and bottom view in (b), from Gibanica et al. (2018). Circle markings indicate accelerometer locations and the rectangular marking indicate a sensor and input force position. The forces were normal to the surface, with a direct accelerance accelerometer sensor configuration.

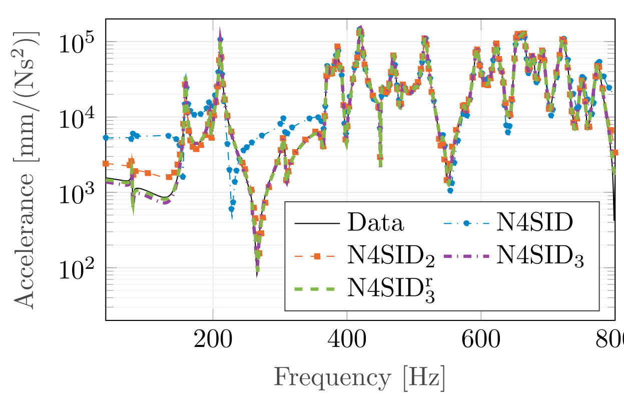

Fig. 2. Magnitude of sum of all FRF channels.

with $\angle$ denoting the complex argument. This channel has the poorest fit for N4SID with NRMSE of $\xi_{14,14} = -4.29$. A vast improvement is seen for the models N4SID$_3$ and N4SID$_3^\mathrm{r}$ with NRMSE of $\xi_{14,14} = 0.98$.

In Fig. 5 the singular values of $\boldsymbol{D}_\mathrm{r}$ is shown. It can be seen that the singular values drop with the addition of residual pseudo system states, and especially the singular values above $m_\mathrm{r} = 6$. This is expected as the model includes more residual effects. It can also be seen that the rank constraint does not affect the remaining singular values.

4. CONCLUSION

A procedure for model identification using N4SID on MIMO accelerance data with physically motivated residual

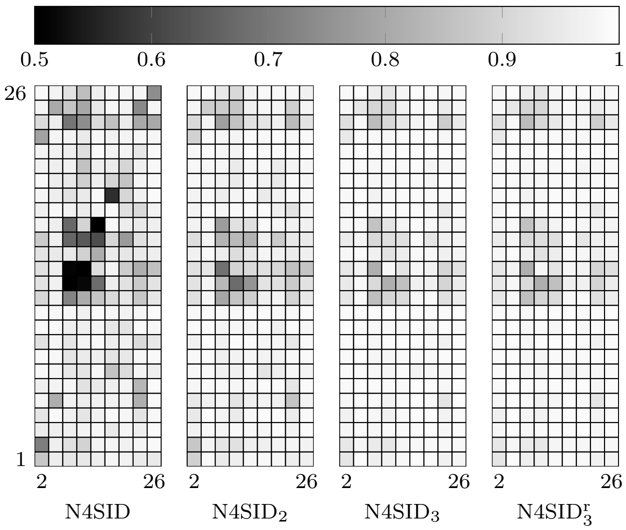

Fig. 3. NRMSE for all channels of the 4 models, with ordered inputs, see Fig. 1.

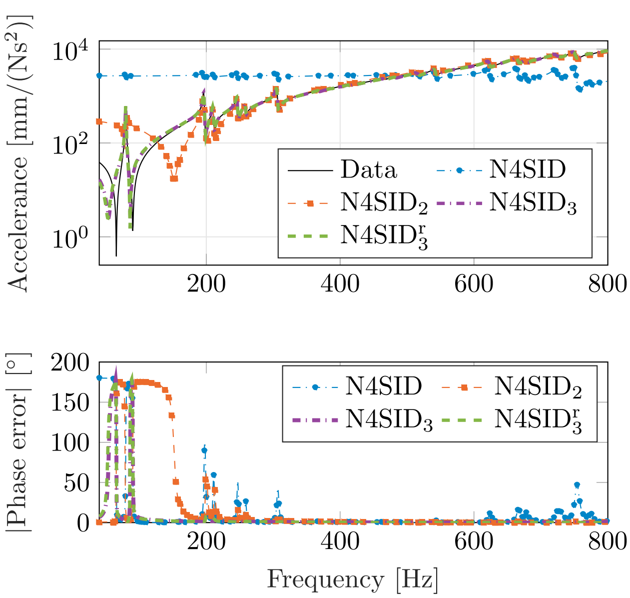

Fig. 4. Direct accelerance for channel 14 of the 4 models.

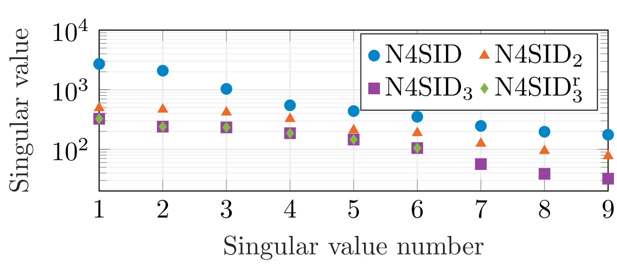

Fig. 5. Singular values of $\boldsymbol{D}_{\mathrm{r}}$ for the four models.

states is presented. The method outperforms models without residual states or models with only mass and stiffness residuals. It is also shown that for truncated models, such as generally obtained from N4SID applied to real test data, a rank constraint on the rigid body mode partition of the direct throughput matrix is necessary for physical consistency. The rank constrain is enforced in the re-estimation of the $\boldsymbol{B}, \boldsymbol{C}$ and $\boldsymbol{D}$ matrices, and is shown to not negatively affect the identified model fit to a significant degree.

ACKNOWLEDGEMENTS

Volvo Car Corporation is gratefully acknowledged for providing the funding for this paper.

REFERENCES

Abrahamsson, T.J.S. and Kammer, D.C. (2015). Finite element model calibration using frequency responses with damping equalization. *Mechanical Systems and Signal Processing*, 6263, 218–234. doi: 10.1016/j.ymssp.2015.02.022.

Ewins, D.J. (2000). *Modal Testing: Theory, Practice and Application*. Wiley-Blackwell, Baldock, Hertfordshire, England; Philadelphia, PA, 2nd edition.

Gibanica, M. and Abrahamsson, T.J.S. (2017). Parameter Estimation and Uncertainty Quantification of a Subframe with Mass Loaded Bushings. In R. Barthorpe, R. Platz, I. Lopez, B. Moaveni, and C. Papadimitriou (eds.), *Model Validation and Uncertainty Quantification, Volume 3*, Conference Proceedings of the Society for Experimental Mechanics Series, 61–76. Springer International Publishing.

Gibanica, M., Abrahamsson, T.J.S., and Allemang, R.J. (2018). Residual states for modal models identified from accelerance data. In *Proceedings of the 36th IMAC*. Orlando, FL, USA. In press.

Gumussoy, S., Ozdemir, A.A., McKelvey, T., Ljung, L., Gibanica, M., and Singh, R. (2018). Improving linear state-space models with additional iterations. In *18th IFAC Symposium on System Identification, SYSID 2018*. Stockholm, Sweden. In press.

Horn, R.A. and Johnson, C.R. (2012). *Matrix Analysis*. Cambridge University Press, New York, NY, 2nd edition.

Kailath, T. (1980). *Linear Systems*. Prentice-Hall, Inc., Englewood Cliffs, N.J, 1st edition.

Liljerehn, A. (2016). *Machine Tool Dynamics - A constrained state-space substructuring approach*. Doctoral thesis, Chalmers University of Technology.

Ljung, L. (1999). *System Identification: Theory for the User*. Prentice Hall, Upper Saddle River, NJ, 2nd edition.

McKelvey, T., Akcay, H., and Ljung, L. (1996). Subspace-based multivariable system identification from frequency response data. *IEEE Transactions on Automatic Control*, 41(7), 960–979. doi:10.1109/9.508900.

McKelvey, T. and Reza Moheimani, S.O. (2005). Estimation of phase constrained MIMO transfer functions with application to flexible structures with mixed collocated and non-collocated actuators and sensors. *IFAC Proceedings Volumes*, 38(1), 219–224. doi: 10.3182/20050703-6-CZ-1902.00037.

Sjövall, P. and Abrahamsson, T. (2007). Component system identification and state-space model synthesis. *Mechanical Systems and Signal Processing*, 21(7), 2697–2714. doi:10.1016/j.ymssp.2007.03.002.

Sjövall, P., McKelvey, T., and Abrahamsson, T. (2006). Constrained state-space system identification with application to structural dynamics. *Automatica*, 42(9), 1539–1546. doi:10.1016/j.automatica.2006.04.021.